Flight-Like Ground Demonstrations of Precision Maneuvers for Spacecraft Formations

Daniel P. Scharf*, Fred Y. Hadaegh†, Jason A. Keim‡, Arin C. Morfopoulos§, Asif Ahmed¶, Yan Brenman‖, Ali Vafaei**, Joel F. Shields¶, Charles F. Bergh††, and Peter R. Lawson‡‡

Jet Propulsion Laboratory, Pasadena, CA 91109

USA California Institute of Technology

Synchronized formation rotations are a common maneuver for planned precision formations. In such a rotation, attitudes remain synchronized with relative positions, as if the spacecraft were embedded in a virtual rigid body. Further, since synchronized rotations are needed for science data collection, this maneuver requires the highest precision control of formation positions and attitudes. A recently completed, major technology milestone for the Terrestrial Planet Finder Interferometer is the high-fidelity, ground demonstration of precision synchronized formation rotations. These demonstrations were performed in the Formation Control Testbed (FCT), which is a flight-like, multi-robot formation testbed. The FCT is briefly introduced, and then the synchronized rotation demonstration results are presented. An initial error budget consisting of formation simulations is used to show the connection between ground performance and TPF-I flight performance.

I. Introduction

In 1967 the Kosmos 186 and 188 spacecraft autonomously rendezvoused,[a] thereby becoming the first autonomous distributed spacecraft.[2] Then in 1969 data from US, Soviet, and European Space Research Organization satellites were correlated to study how large solar flares interacted with the Earth's magnetosphere and ionosphere, in turn becoming the first distributed spaceborne sensor.[3] Today, multiple spacecraft formation flying is a critical technology for planned and future missions of NASA,[4–7] ESA[8,9] and other national space and defense agencies.[10–12]

Distributed spacecraft missions require varying levels of inter-spacecraft coupling. We define a *formation* as a group of independent spacecraft with a subset of dynamic states coupled by automatic feedback control such that a direct or indirect coupling exists between any pair of spacecraft. In a formation, if the state of any spacecraft changes unexpectedly, then at least one other spacecraft reacts.

The technology road map for the formation-flying Terrestrial Planet Finder Interferometer (TPF-I),[13] a multi-spacecraft interferometer for direct exoplanet detection and characterization, identifies several key milestones. In particular, the Formation Control Testbed (FCT) will demonstrate at the system-level an autonomous synchronized formation rotation through 90 deg. with a portion of the rotation having relative position control of $\leq 5.0\,cm$ RMS and attitude control of $\leq 6.7\,arcmin$ RMS. These requirements were derived from system-level error budgets that account for the increased terrestrial disturbance environment. In addition, to demonstrate the flexibility of onboard path-planning, two synchronized rotation profiles are to be demonstrated. Finally, for each profie, these performance requirements must be met three times with at least two days between each demonstration. This temporal requirement ensures that the technology capability developed is robust and repeatable.

The primary contribution of this paper is to report the completion of these demonstration rotations, as confirmed by a NASA independent review board, and describe the experimental results. The following section overviews the FCT. Then the synchronized formation rotation maneuver is summarized as well as the onboard formation guidance algorithm for generating spacecraft trajectories. The formation control

*Senior Engineer, Guidance & Control Analysis Group, 4800 Oak Grove Dr. M/S 198-326, AIAA Member.
†Senior Research Scientist, Guidance & Control Analysis Group, AIAA Fellow.
‡Staff Engineer, Guidance & Control Analysis Group, AIAA Member.
§Staff Engineer, Robotic Hardware Systems Group.
¶Senior Engineer, Guidance & Control Analysis Group.
‖Software Engineer, Flight Software, Operating Systems & Avionics Interfaces Group.
**Associate Engineer, Guidance & Control Analysis Group.
††Senior Engineer, Robotic Hardware Systems Group.
‡‡TPF-I Systems Manager, Optics Section Technical Staff.

[a]The IGLA relative sensor used for this rendezvous appears to have supported only "straight-in" maneuvering.[1] That is, the spacecraft would be maneuvered to face one another, and the chaser would fly straight at the target feeding back line-of-sight variation. From a general formation flying perspective, it is not clear at what distance the automatic system was engaged, and it does not appear that maneuvers such as circumnavigation (cf. the KURS relative sensor flown today[2]) were possible.

architecture is also discussed. Next, the experimental results for the formation rotations are given and an initial error budget tieing ground performance to flight performance. Finally, we summarize and present some future directions.

II. The Formation Control Testbed

The Formation Control Testbed (FCT) is a multi-robot, flight-like, system-level testbed for ground validation of formation GNC architectures and algorithms, including autonomous rendezvous and formation infrastructure technologies such as communication protocols and formation sensors.[14,15] The FCT currently consists of two robots with flight-like hardware and dynamics, a precision flat floor that the robots operate on, ceiling-mounted artificial stars for attitude sensing and navigation, and a "ground control" room for remotely commanding the robots and receiving telemetry. A third robot is planned. The robots and part of the flat floor are shown in Figure 1. The FCT was designed and built in cooperation with industry partners Guidance Dynamics Corporation, Di-Tec International, and Applied Control Environments, Inc.

A detailed view of a robot with specific hardware identified is given in Figure 2. Each robot has a lower

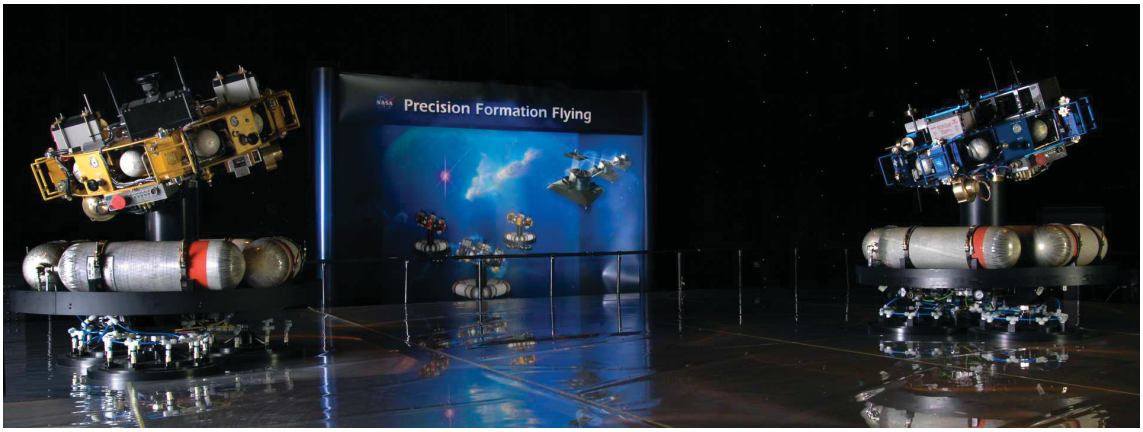

Figure 1. Formation Control Testbed Operations Area with Two Robots.

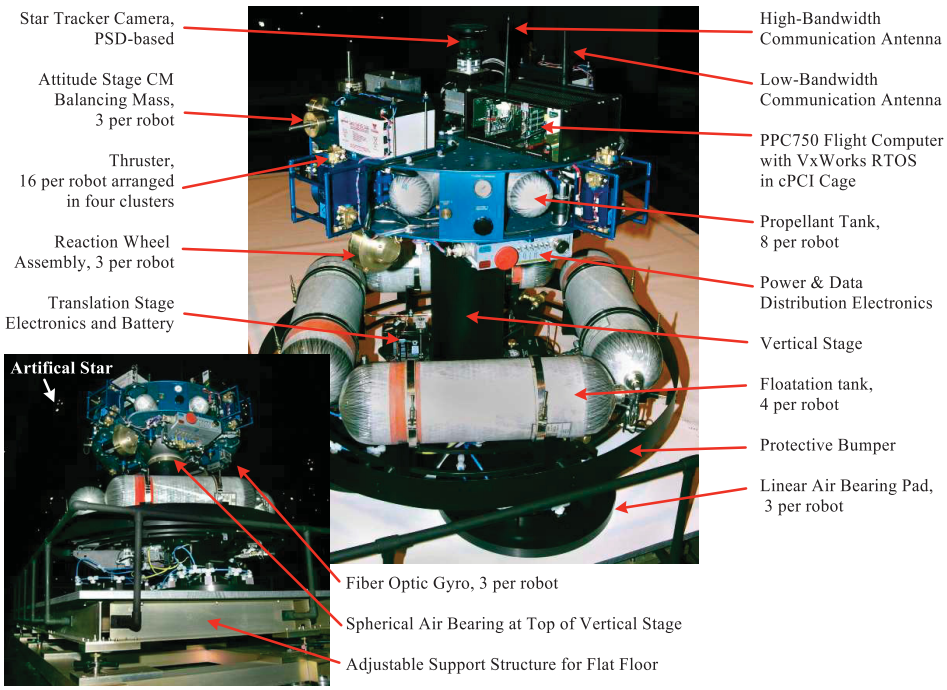

Figure 2. Major Components of an FCT Robot.

translational stage (TS) and an upper attitude stage (AS). The AS is the spacecraft emulator, and it is completely disconnected from the TS. The attitude stages are shown tilted in Figure 1. Each AS houses avionics, spacecraft actuators, sensors, inter-robot and ground-to-robot communication antennas, and the spacecraft processors. With reference to Figure 2, the TS provides both translational and rotational degrees of freedom to the attitude stage by means of (i) linear air bearings that float an entire robot on a cushion of air a few thousandths of an inch thick, and (ii) a spherical air bearing in which a spherical surface on the bottom of the AS floats on a cushion of air generated in a pressurized cup at the top of the TS. Telescoping vertical stages with tens-of-centimeters of travel are being installed to provide the translational degree of freedom normal to the flat floor. See Figure 3.

The FCT is housed in the former Celestarium at JPL, which has a $12.2\,m$-diameter floor space and a $7.6\,m$ high, dome-like ceiling. The $7.3\,m$ x $8.5\,m$ flat floor of the FCT consists of fourteen, $1.2\,m$ x $3.7\,m$ metal panels. Each panel is ground to a smoothness of a few thousandths of an inch and mounted on a support structure that has coarse and vernier leveling screws. Periodic laser surveys of the floor are used to level the floor panels and ensure acceptable step sizes between panels.

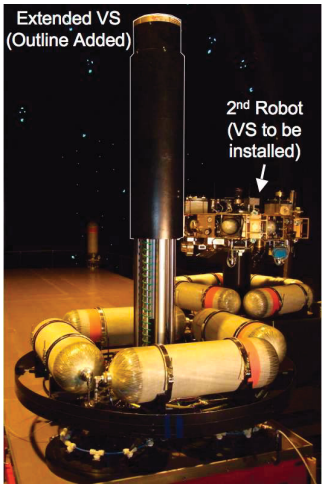

Figure 3. Vertical Stage Installation.

Each robot has an onboard PPC750 single board computer for the Formation and Attitude Control System (FACS) software.[16] All attitude and formation algorithms are run onboard; only commands are up-linked to the robots. The FACS is encapsulated by a Software Executive (SE) that provides a flight-like environment for execution and is designed to support a wide variety of control architectures and algorithms. The SE also provides command and telemetry handling, device-level communication, inter-spacecraft communication, inter-vehicle clock-offset estimation, control cycle synchronization, and scheduling within the real-time VxWorks operating system.[17] The actuators on each robot consist of sixteen thrusters with $0.5 - 22\,N$ thrust range arranged symmetrically in clusters of four and three reaction wheel assemblies (RWAs). The thrusters have a minimum on-time of $6\,ms$ and a specific impulse of $55\,s$. Each RWA is capable of delivering $0.2\,Nm$ and storing $1.4\,Nms$.

Each robot has typical, single-spacecraft attitude sensors and avionics. The attitude sensors consist of three, orthogonally-mounted KVH DSP-3000 fiber optic gyros and a pseudo-star tracker. The star tracker measures the directions to strobed, infra-red beacons that are mounted on the ceiling of the FCT and function as artificial stars. Since the stars are in the near-field, both position and attitude with respect to the star frame can be determined. The quaternion and position measurements are separated in the avionics and fed to the flight computer as the output of a star tracker and a GPS-like position sensor. The per axis standard deviations of the star tracker attitude and position measurements are arc minute- and subcentimeter-level, respectively. The star tracker and gyro measurements are combined in a Kalman-based attitude estimator, which accounts for the Earth's rate of rotation.

For a formation to couple translational degrees-of-freedom, spacecraft must estimate relative positions. Relative position knowledge can be obtained from direct relative measurements or by differencing positions with respect to a common reference point. Communicating and differencing GPS-derived positions is an example of the latter.[18] The FCT currently uses the this approach. The SEs on each robot read the pseudo-GPS measurement from the avionics and broadcast it. The SEs then difference their local measurements with the broadcast measurements and pass this relative measurement to the FACS. This SE interface emulates omni-directional sensors for deep space formations, such as the Formation Acquisition Sensor.[19]

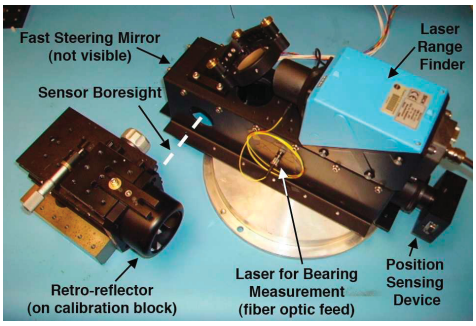

Figure 4. The Optical Pointing Loop.

The direct relative sensor being developed for the FCT is shown in Figure 4 and is called the Optical Pointing Loop (OPL). Conceptually, a laser diode, fast steering mirror (FSM), and position sensing device on one robot are used to keep the laser diode beam centered on a corner cube mounted on another robot. The relative bearing is given by the angular position of the FSM. A co-sighted SICK DML40-1111 laser range finder provides range.

III. Formation Rotation Guidance and Control

Having reviewed the FCT, now the specific maneuver being demonstrated is discussed, including the onboard algorithm that generates the formation trajectories that the robots follow in real-time and the feedback control loops used to do so.

III.A. Formation Control Architecture

For small-to-medium formations, the Leader/Follower (L/F) formation architecture is effective.[20] In L/F, the control couplings among spacecraft in a formation are hierarchical. Each follower spacecraft, which can also be a leader for another, controls with respect to a subset of other vehicles. This subset typically contains only one craft. Necessarily, there is at least one spacecraft that follows no one. The hierarchical structure leads to straightforward stability conditions based on the stability of a follower's tracking law. For the current two robots of the FCT, an L/F architecture is implemented in the FACS. The Follower controls its position relative to the Leader, and the Leader applies feedforward forces.

III.B. Formation Drift Controller

Formation control is concerned with relative positions. An additional, outer control loop is needed for the inertial position of a formation. For example, for a formation in LEO, the formation control loop would maintain, say, a tetrahedral configuration, while an outer orbit control loop maintains the overall orbit of the formation. This outer loop in the FCT is called the Formation Drift Controller (FDC). It is a low-authority controller that maintains the geometric center of the formation at a specified point within the FCT. To prevent interference with the formation control loops, a single robot collects inertial position data, determines a translational impulse to apply to the formation, and broadcasts this impulse to all formation members. Then the robots execute the impulse simultaneously. Since the same impulse is applied simultaneously by all formation members, the relative position dynamics, that is, the formation dynamics, are not affected.

III.C. Specification of Synchronized Rotation

The design of TPF-I has evolved through various planar configurations to the current tetrahedral configuration. In each design, however, the formation must rotate as a virtual rigid body about an axis perpendicular to the plane defined by the collecting spacecraft, which are referred to as collectors. Collectors direct light to a combiner spacecraft. The location of the rotation axis with respect to the collector-plane is free and is generally chosen based on a metric of optimality.[21] In earlier TPF-I designs, thruster quiescent windows were necessary for data collection: thruster-induced vibrations would disrupt subnanometer optical tracking loops in the payload. Due to this quiescence constraint, the spacecraft travel on polygonal approximations to circles during a formation rotation. Then periodic thruster firings direct the spacecraft onto the next side of the polygon. Also, even if throttleable thrusters, such as ion thrusters, are used, the finite duration of the digital control cycle results in spacecraft traveling on a polygon as well. In this case, of course, the polygonal approximation is much finer. For either type of thruster, the polygonal approximation may be characterized by the angular chord width θ. See Figures 5 and 6.

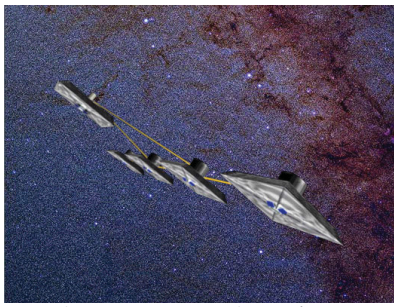

Figure 5. TPF-I Linear Array.

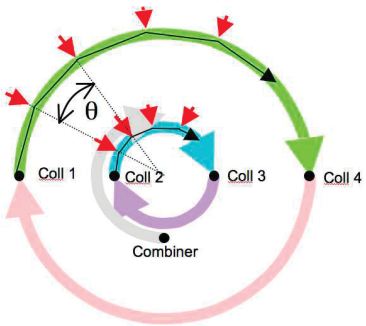

Figure 6. Example of Polygonal Approximations in Formation Rotation of TPF-I Linear Array. Arrows indicate thruster firing windows. "Coll" stands for collector spacecraft.

Five parameters specify a formation rotation: angular chord width θ, rotation axis λ, rotation rate ω, rotation angle ϕ, and vehicle separation b (for baseline). The values of these parameters for FCT demonstrations are derived from the TPF-I Technology Road Map, testbed requirements levied during the FCT development reviews, and system-level error budgets. The FCT rotation requirements are given in Table 1.

An example maneuver with $\theta = 40$ deg. is shown in Figure 7. There is a transient spin-up regime and a performance regime. The performance regime consists of one chord plus a quarter chord on either side. The performance regime shows that the formation can transition onto and off of chords while maintaining performance. Additionally, the white thruster clusters on each robot, which lie on the initial inter-robot vector, must remain pointed at the other robot. That is, the robots translate and rotate in synchrony.

Table 1. FCT Rotation Requirements.

Parameter	Value	Note
θ	20, 40 deg.	To show flexibility
λ	[0 0 1]	FCT currently 5DOF
ω	5 arcmin/s	10x flight rate
ϕ	90 deg.	Per Tech. Road Map
b	3.4 m	From error budgets

III.D. Synchronized Rotation Guidance Algorithm

To show a system-level capability, the FCT robots must be commanded and operated as a formation. In particular, a single high-level command initiates autonomous, onboard path-planning and execution of a formation rotation. Except for the baseline b, this command specifies the parameters of Table 1. The baseline for a formation rotation is the current stored baseline value. The baseline value is updated by commanding a formation reconfiguration, which moves spacecraft from one static configuration to another along collision-free trajectories.[22] An example command for a synchronized rotation is

```
facs_cmd GUID_FORM_SYNCH_ROT time {450} Rotation {0.0,0.0,-2.0944} Duration {1440} LinArcLen {0.6982}
```

A TCL-based interpreter in the SEs processes this command: `facs_cmd` is a keyword for this interpreter, `GUID_FORM_SYNCH_ROT` is a keyword for the sub-interpreter within the guidance software module, `time` specifies the rotation start time, `Rotation` is $\phi \cdot \lambda$; `LinArcLen` is θ, and `Duration` is ϕ/ω.

The guidance architecture is hybrid. Specifically, the Leader calculates all translational commands and relays them to the Follower(s) each time step. Attitude commands, however, are calculated by each spacecraft based on high-level parameters that are also sent by the Leader each time step. This architecture was initially chosen to provide deterministic communication requirements.

Figure 8 shows a schematic of the translational trajectory generated by the guidance algorithm. This schematic is for a single spacecraft relative to the point of formation rotation. The rotation point is chosen to minimize the integral of the energy expended during the formation rotation. For the FCT, both robots apply feedforward accelerations to rotate about the geometric center of the formation. The example schematic shows four, 40 deg chords. The translational rotation trajectory consists of (i) initial and final tangential acceleration stages, shown in green, to start and stop the formation, (ii) constant speed, coast portions along chords, shown in black, and (iii) constant speed, rounded corners, shown in blue that are effected by constant normal acceleration. The acceleration stages, both tangential in green and normal in blue, use the maximum translational acceleration for path planning, which is a parameter specified within the guidance software. For these demonstrations it is $3\,mm/s^2$. The chord coasting speed and the unique turn radius r are solved for given this maximum acceleration, the angular chord width, the inter-robot separation b, and the maneuver time T. The resulting relative speed is approximately

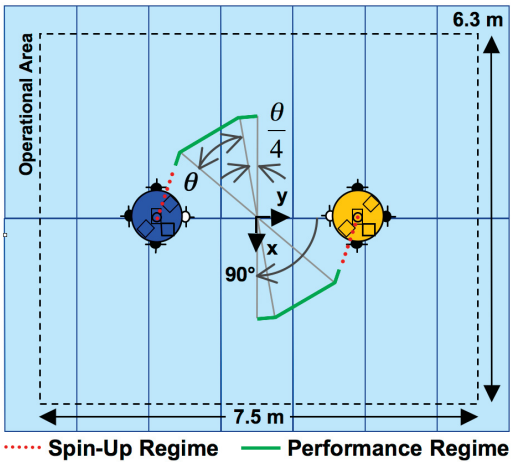

Figure 7. Schematic of formation rotation in the FCT with parameters of Table 1.

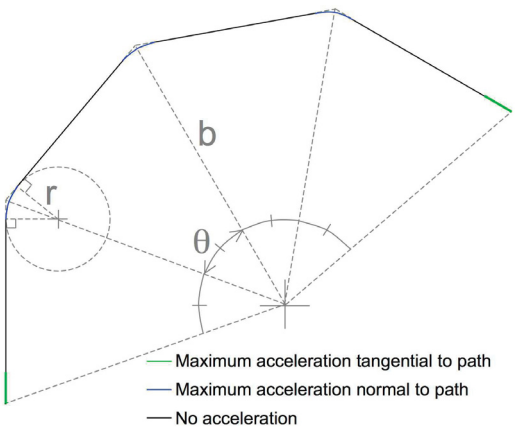

Figure 8. Schematic of formation rotation trajectory used by FACS guidance algorithm.

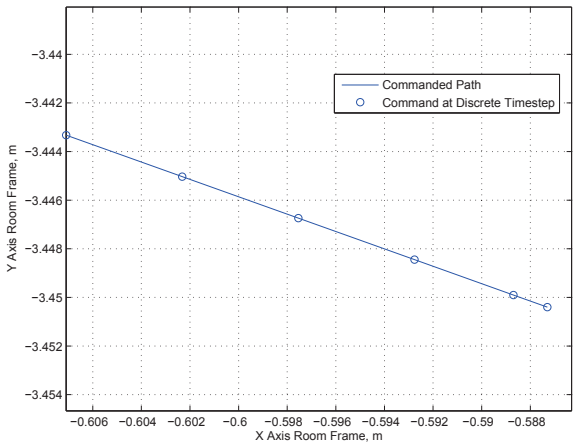

Figure 9. Formation Guidance Relative Position Command at Start of Synchronized Rotation.

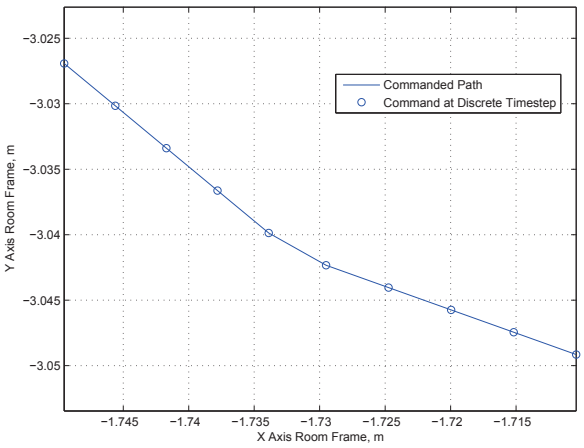

Figure 10. Formation Guidance Relative Position Command at Chord Transition of Synchronized Rotation.

$5\,mm/s$ for both 20 and 40 deg angular chord widths. Figures 9 and 10 show example commands for the FCT robots at the start and at the first chord transition. The tangential acceleration phase can be seen in Figure 9, during which the distance between subsequent positions grows. The rounded corner can be seen in Figure 10. For scale, the arc length of rounded corner (the blue portions in Figure 8) is $3\,mm$.

The synchronized rotation attitude commands are derived from two pointing constraints. The second constraint depends on the relative position command. First, a primary body vector is aligned with a primary inertial vector, such as a telescope boresight with the direction to the target star. Then, a secondary body vector is aligned as much as possible with the direction to a specified neighboring spacecraft. When primary and secondary vectors are orthogonal, as is the case for TPF-I and FCT, and when there are only two vehicles as currently in the FCT, the attitude command aligns body-fixed vectors on both robots with the commanded inter-robot vector. Note that since the robots travel on chords, the angular velocity needed to keep a body-fixed vector aligned with the inter-robot vector is not constant. The formation guidance accounts for this variation.

IV. FCT Demonstrations

For each demonstration, the robots are maneuvered independently to starting positions and shut-down. Then the robots are re-started and go through their single-spacecraft check-out modes. During these check-outs, a command script is sent to each robot. Each command includes its activation time. After these check-outs, each robot has established inertial attitude control and independent, inertial position control using their gyros and star trackers. The command for formation initialization then activates. During formation initialization, independent, inertial translational control loops are disabled, the robots establish communication, synchronize control cycles, and point specified body vectors at one another. At the end of formation initialization, the robots automatically reconfigure to their current configuration which activates the formation control loop. Then the command for formation rotation activates. Beginning at the end of formation initialization, the relative position is fed back for formation control.

For all demonstrations, the gold Robot 1 (R1) is the Leader, and the blue Robot 2 (R2) is the Follower. The next series of figures shows data from one of the six synchronized rotation demonstrations for which the angular chord width θ is 20 deg. Figure 11 shows an example of the inertial motion of two robots during a 100 deg formation rotation. While only 90 degrees are required, an integer number of chords is commanded that results in a rotation greater than or equal to 90 deg. The motion of the geometric center of the formation shows that the formation as a whole drifts due to floor slope and that the FDC keeps the formation relatively stationary. The initial motion of R2 counter to the rotation direction is due to a decaying transient from the automatic reconfiguration. The chords that the robots move on are not apparent in Figure 11. To see the chords, relative motion must be considered. Figure 12 shows the motion of the R2 relative to R1 derived from the inertial motion of Figure 11. Both the estimated relative position and the commanded relative position are shown. Now the five, 20 deg chords are apparent. Recall that the performance regime consists

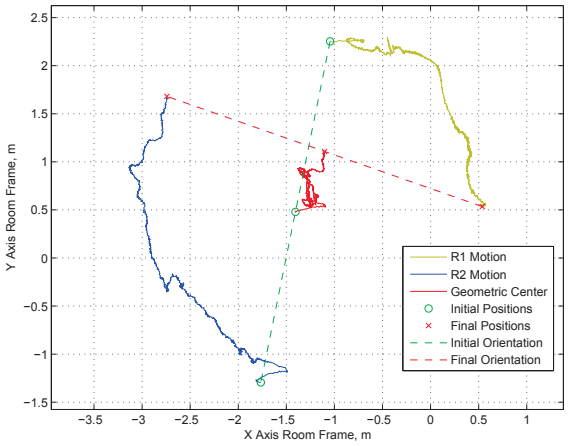

Figure 11. Inertial Motion of an Synchronized Rotation Demonstration.

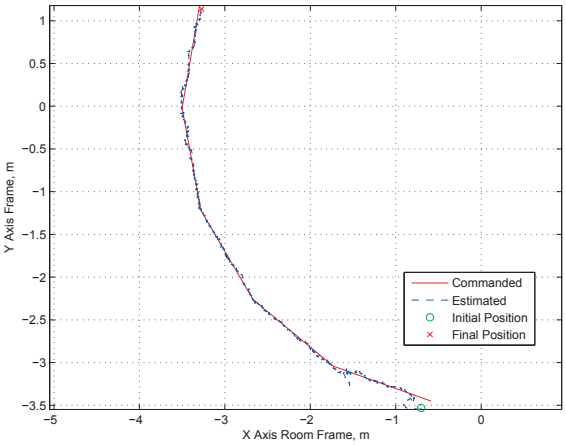

Figure 12. Relative Motion of Demonstration Corresponding to Figure 11.

of one full chord plus the bordering quarter-chords. Since there are five chords, there are three possible performance regimes. When multiple performance regimes satisfy the performance requirements, the regime with the best performance is selected. However, for an angular chord width of 40 deg, there are only three chords, and hence only one possible performance regime.

Figure 13 shows the formation tracking error per axis during the performance regime of Figure 12, which consists primarily of the fourth chord. The tracking error is essentially $\pm 5\,cm$. The performance requirement is that the RMS per axis be less than or equal to $5\,cm$. Also shown in Figure 13 are dashed lines indicating the RMS values for each axis and the RMS requirement. Since the blue and green dashed lines fall within the cyan dashed line, the performance requirement is met. Finally, Figure 13 also includes dashed, black vertical lines to indicate inter-robot communication interruptions. The times of these drops are included in subsequent telemetry. Due to the hybrid guidance architecture, when communication is interrupted, the Follower must assume a formation command. For simplicity, the Follower currently copies that last valid command. Figure 14 shows the worst communication interruption that occurred during the demonstrations. On average, one timestep of communication was interrupted every $60\,s$. Despite interruptions, performance is maintained by the formation control loop.

Considering attitudes, Figure 15 shows select inertial positions from Figure 11, the instantaneous relative position vector, and the instantaneous attitude of each robot. The attitude is shown by rotating a fixed

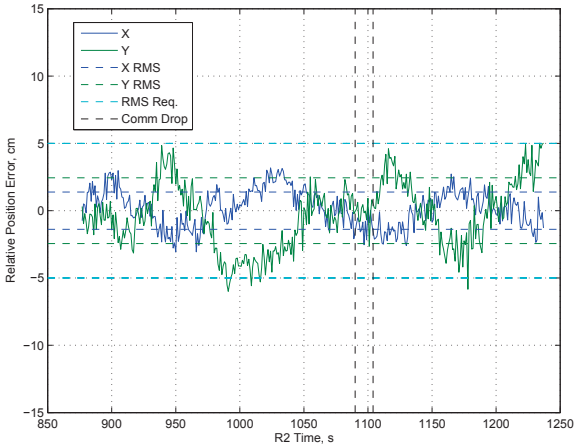

Figure 13. Formation Tracking Error During Performance Regime of Figure 12. Also included are the scalar RMS values for each axis indicated by dashed horizontal lines, the RMS requirement, and the times of communication interruptions.

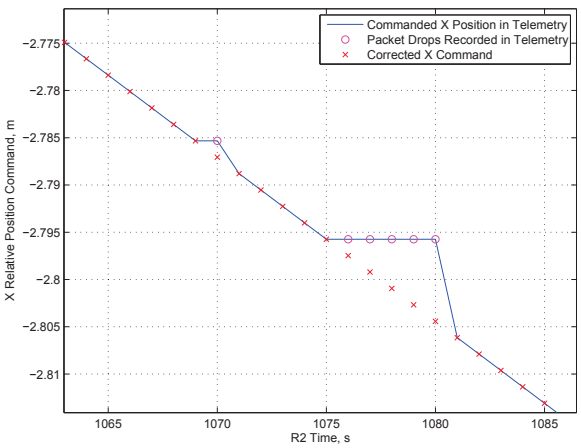

Figure 14. X Axis Guidance Command on Follower During Worst Inter-Robot Communication Interruption. The solid blue line is relative position command on Follower. Circles indicate communication drops recorded in telemetry. Red x's indicate what the x-axis command would have been with uninterrupted communication.

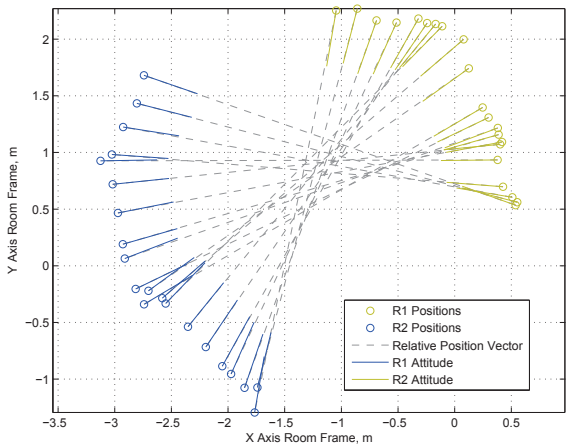

Figure 15. Planar Attitudes of Robots for Select Inertial Positions from Figure 11.

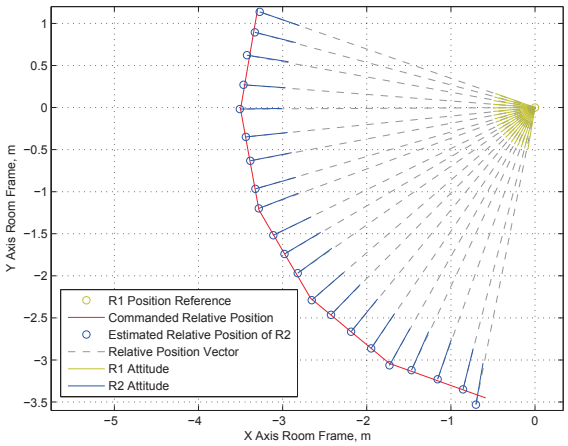

Figure 16. Planar Attitudes of Robots as a Function of Relative Position for the Inertial Positions of Figure 15.

body-vector into the inertial frame via the attitude command recorded in telemetry. With reference to Figure 7, the body vector for each robot is the vector from the center of a robot to its white thruster cluster. Hence Figure 15 shows that the robots are synchronizing their attitudes with their relative position. To see the attitude synchronization as the robots move along chords, Figure 16 shows the attitudes as a function of relative position.

Similar to the translational discussion, Figures 17 and 18 show the Leader's and Followers attitude errors versus time. The attitude errors in each axis are the angles that a robot must rotate about each respective body axis to reach the commanded attitude. RMS values and the RMS requirement of $6.7\,arcmin$ are also shown in these figures. Again, only horizontal dashed lines should be compared for evaluating the performance. For example, even though the X- and Y-axis errors in Figure 18 often exceed the $6.7\,arcmin$ RMS requirement lines (the cyan dashed line), the Follower meets its performance requirement: the blue and green dashed lines fall within the dashed cyan lines. The black, vertical dashed lines again indicate interruptions to inter-robot communication. Since packet drops do not affect the Leader, packet drops are not shown in Figure 17.

The Follower's attitude error is larger because of residual thruster misalignments. The thruster calibration accuracy is limited by $\pm 30\,deg$ tip/tilt limit of the spherical air bearings on the FCT robots. This angular limit in turn constrains the duration of calibration data that can be collected. Since the Follower thrusts more to control relative position, the residual misalignments induce larger disturbance torques. With further calibration, the Follower's attitude performance should approach the Leader's performance of essentially $\pm 7\,arcmin$.

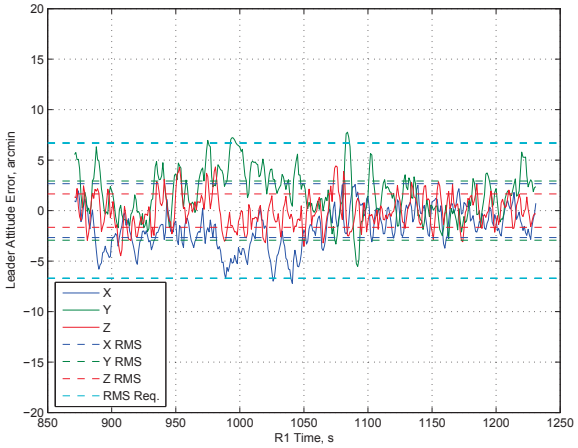

Figure 17. Leader Attitude Error During Performance Regime of Figure 12.

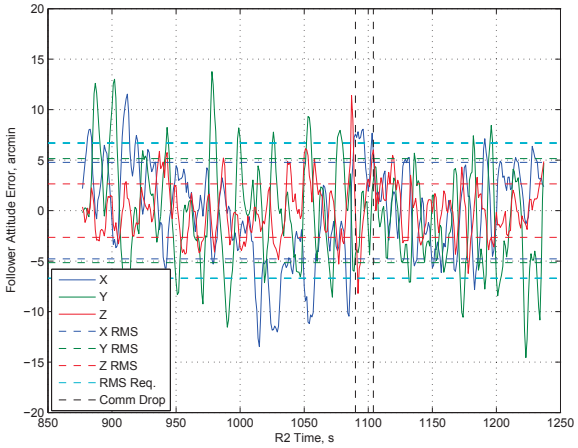

Figure 18. Follower Attitude Error During Performance Regime of Figure 12.

Table 2 summarizes the six synchronized rotation demonstrations that were performed. All performance criteria were met. The attitude and formation performance shown in Figures 13, 17, and 18 are for Demonstration 3. The attitude and formation performance for the five other cases are shown in Appendix A. Some trends are apparent. First, relative translation errors are generally within $\pm 5\,cm$ with occasional departures to $8-10\,cm$. The worst departure was to $13\,cm$. These departures result from the robots encountering new differential floor slopes, particularly when crossing the seams between panels of the flat floor. Construction, including drilling into bedrock, was occurring adjacent to the FCT during these demonstrations. This drilling caused day-to-day floor variations that generally increased disturbance levels. During $\theta = 20\,deg$ performance regimes, each robot would cross one or two floor seams, and for $\theta = 40\,deg$, each would cross two or three floor seams. These crossings were largely in the y-direction. Therefore, the formation encounters the least disturbance for $\theta = 20\,deg$ and along the x-axis. This category had the best performance of better than $1.5\,cm$ RMS.

Whereas the worst formation performance during these demonstrations was $4.6\,cm$ RMS, the limiting factor for formation performance was the *attitude* performance requirement. As the non-DC "gain" of the formation control law was increased, the Follower's attitude performance would degrade due to increased disturbance torques resulting from residual thruster misalignments. The control design trade-off was then to maximize the integrator gain for formation control while maintaining a modest non-DC gain to meet the attitude performance requirement. Integrator rate and magnitude saturations were necessary. The lightly-damped oscillations that can be seen in the $\theta = 40\,deg$ formation error data in Appendix A are due to reducing the integrator rate limit to obtain a shorter integrator response time. Since the attitude requirement limited the performance of the formation control system and construction increased disturbance levels, the majority of performance numbers in Table 2 do not reflect the ultimately achievable performance of the FCT. In particular, the x-axis formation control performances of $< 1.5\,cm$ RMS are approaching the limit expected due to sensor noise.

Table 2. Summary of FCT Synchronized Formation Rotation Demonstrations.

Success Criteria	Criteria Values by Demonstration						Required Value
Demonstration ID	1	2	3	4	5	6	N/A
Demonstration Date (m/d/y) & Time	9/18/07 10:48	9/21/07 12:45	9/25/07 10:43	9/13/07 18:57	9/24/07 10:48	9/26/07 20:04	N/A
Relative Position RMS Error, cm	Formation Control Performance						
X	1.49	1.43	1.36	2.89	2.46	2.76	≤ 5
Y	4.50	2.41	2.44	4.61	4.29	4.36	≤ 5
R1 Attitude Error RMS, arcmin	Rotational Control Performance - Leader						
X	2.31	3.14	2.67	3.70	2.62	2.16	≤ 6.7
Y	2.40	3.49	2.93	4.74	2.96	2.71	≤ 6.7
Z	1.98	1.84	1.65	3.31	1.74	1.59	≤ 6.7
R2 Attitude Error RMS, arcmin	Rotational Control Performance - Follower						
X	4.48	4.65	4.78	4.71	5.70	4.50	≤ 6.7
Y	6.41	6.28	5.15	5.72	5.70	5.41	≤ 6.7
Z	3.54	2.97	2.65	3.00	3.13	2.80	≤ 6.7
Maneuver	Multiple Guidance Profiles						
Formation Baseline b, m	3.5	3.5	3.5	3.5	3.5	3.5	≥ 3.44
Angle Rotated ϕ, deg	100.0	100.0	100.0	111.4	105.8	106.5	≥ 90
Chord Width θ, deg	20	20	20	40	40	40	= 20, 40
	Repeatability						
Time b/n Runs of Same θ, hr	N/A	74.0	94.0	N/A	225.9	57.3	≥ 48

V. Error Budget for Estimating Flight Performance

The purpose of the preliminary formation error budget is to show a link from the FCT demonstrations at the several centimeter- and several arcminute-level to TPF-I flight requirements at the sub-centimeter and sub-arcminute-level. The approach taken is to identify the key control system parameters, develop a control system simulation environment as a function of these key parameters, show that the simulation environment can qualitatively and quantitatively reproduce the FCT demonstrations for parameter values corresponding to the FCT, and finally, change the parameters to flight values and show the TPF-I flight requirements are satisfied. The exact same control laws are used in both the FCT and TPF-I simulations. Therefore, a link is shown between FCT performance and TPF-I performance by simply varying the key parameters from FCT values to TPF-I values. The key parameters identified for this preliminary error budget are:

- Mass
- Inertia
- Relative Estimate Variance
- Attitude Estimate Variance
- Thruster Magnitude
- Thruster Minimum On-Time
- Thruster Misalignment
- Vehicle Separation
- Formation Rotation Rate
- Angular Chord Width
- Disturbance Magnitude

A simulation environment was developed by extending previous work on TPF-I performance analysis.[16] The extended environment includes:

- Rigid body dynamics,
- Sensor models that add Gaussian noise of the appropriate standard deviations,
- Guidance trajectories from the FCT software,
- Control laws identical to the FCT demonstration control laws,
- The thruster geometry of the FCT, which is representative of a TPF-I flight design,
- A thrust allocation algorithm that converts forces and torques into thruster on-times,
- Actuator models that include minimum thruster on-time and directional misalignments,
- Disturbance models that either emulate floor slope variations or differential solar pressure.

For this analysis, the thruster performance is assumed to not degrade over the duration of a simulation. One advantage of ion thrusters, which are part of the current baseline design,[23] is that force level can be maintained even with thruster degradation.[24] The cost is reduced fuel efficiency on the order of 10-20%, which affects resource budgets but not formation performance. In addition, thruster plumes are assumed to not interact with the spacecraft. Thruster plume interactions have been shown to be negligible due to careful design of thrust directions (e.g., out of the collector plane) and the use of ion thrusters, which have 10-15 deg. divergence angles.[23] In the current environment, communication is error free. The FCT disturbance model consists of differential floor slopes to apply in $20\,s$ intervals during a simulation. Since the levelness of the flat floor varies by up to $0.0004\,in.$, differential floor slope varies between $\pm 0.0008\,in.$ An optimization algorithm fits the differential floor slope magnitude to the observed formation flying errors of an FCT demonstration within this range. All simulations use the same seed for generating sensor noise.

Figures 19-24 show the translational and rotational performance from Demonstration 3 and the output of the FCT simulation error budget. The relative position error agreement is excellent. While the attitude errors agree in magnitude, the simulated errors have higher frequency content. Agreement can be improved in future analyses by including the center-of-mass offset of the FCT attitude stage and reducing attitude sensor noise in the simulation. However, the thruster direction misalignment captures the magnitude difference in the attitude tracking errors of the Leader and Follower.

To show that the FCT simulation environment captures the relevant parameters across FCT demonstrations, the simulation environment was also applied to Demonstration 5. Figures 25 and 26 show the agreement of the relative position error after fitting the disturbance. The attitude errors are similar to the previous cases.

Having shown the simulation error budget reproduces both the qualitative and quantitative behavior of the FCT demonstrations, it is was then applied to TPF-I. In the simulation environment, the parameters of Table 5 were switched from FCT to TPF-I values. Figure 27 shows the relative position trajectory followed in the TPF-I simulation. Then Figures 28-30 show the resulting simulated performance of the TPF-I formation control system. In all cases, TPF-I flight requirements are met with margin.

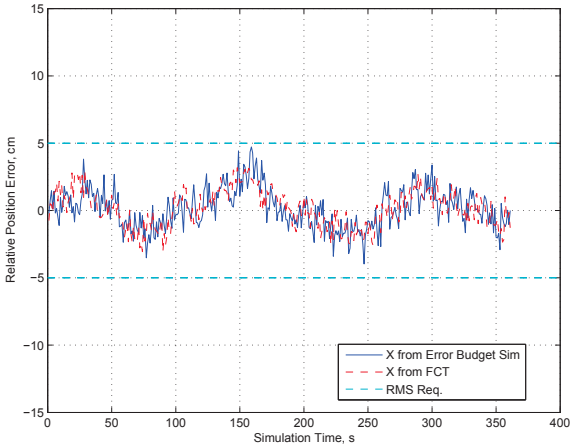

Figure 19. Comparison of Error Budget Simulation with X Axis Formation Error from Demonstration 3.

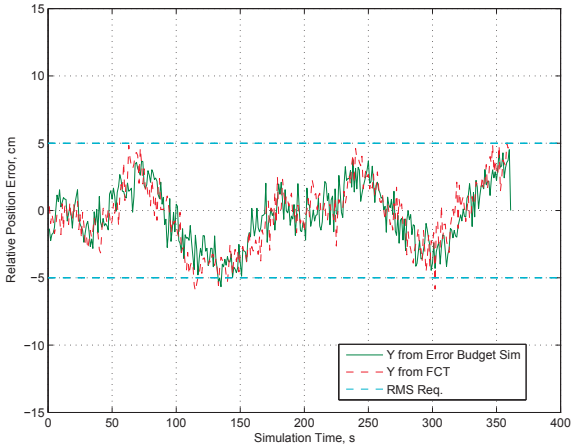

Figure 20. Comparison of Error Budget Simulation with Y Axis Formation Error from Demonstration 3.

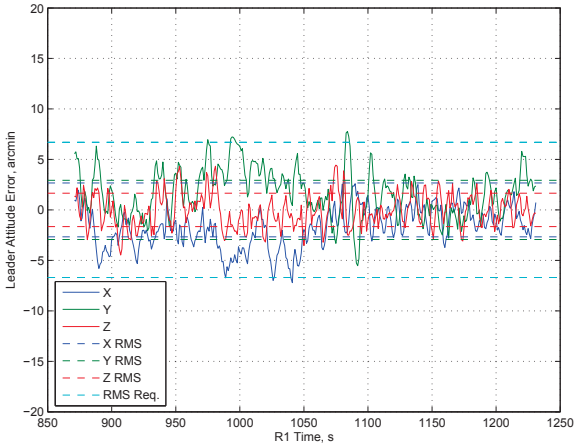

Figure 21. Leader Attitude Error for Demonstration 3 (reproduction of Figure 17).

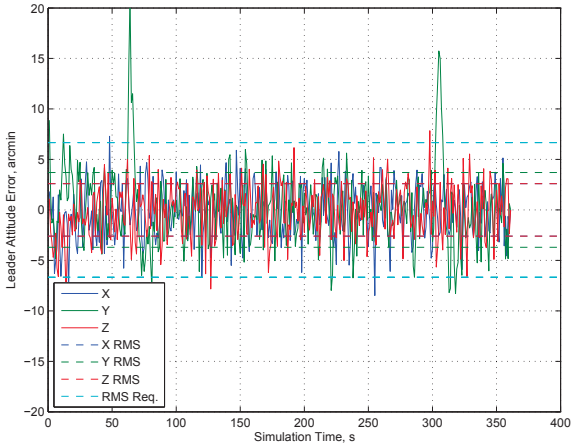

Figure 22. Error Budget Simulation of Leader Attitude Error for Demonstration 3.

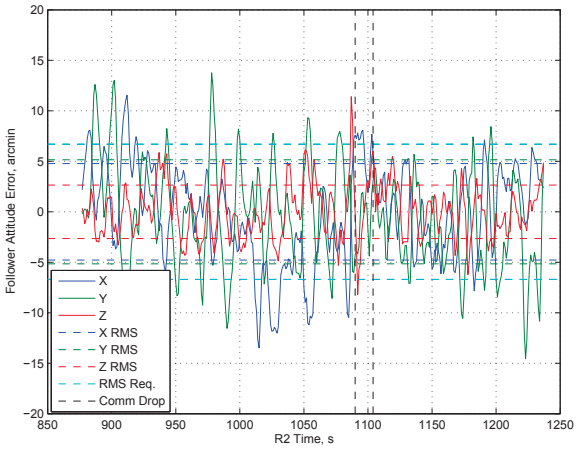

Figure 23. Leader Attitude Error for Demonstration 3 (reproduction of Figure 18).

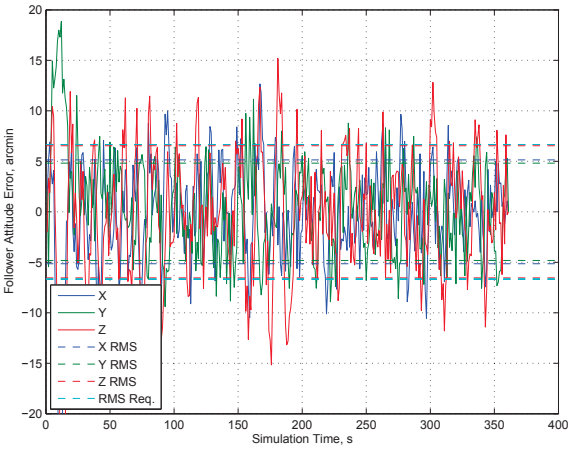

Figure 24. Error Budget Simulation of Follower Attitude Error for Demonstration 3.

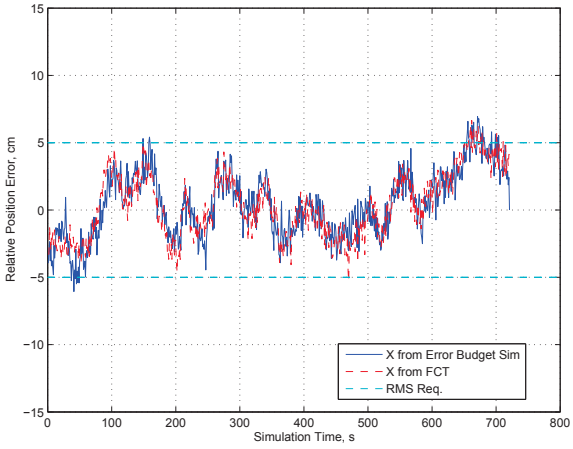

Figure 25. Comparison of Error Budget Simulation with X Axis Formation Error from Demonstration 5.

Figure 26. Comparison of Error Budget Simulation with Y Axis Formation Error from Demonstration 5.

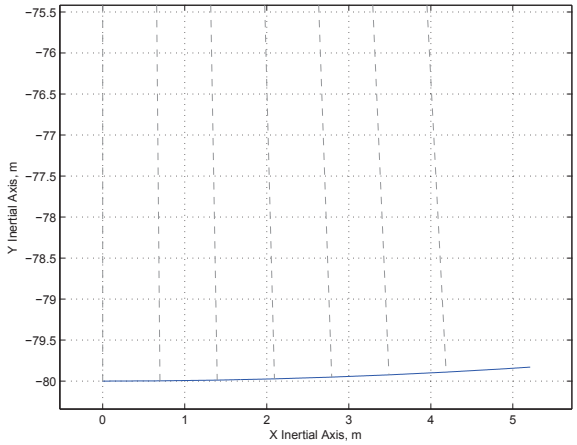

Figure 27. Relative Position Trajectory for TPF-I Error Budget Simulation. Note 80 m separation. This trajectory has six 0.5 deg chords. The grey dashed lines indicate the chord boundaries.

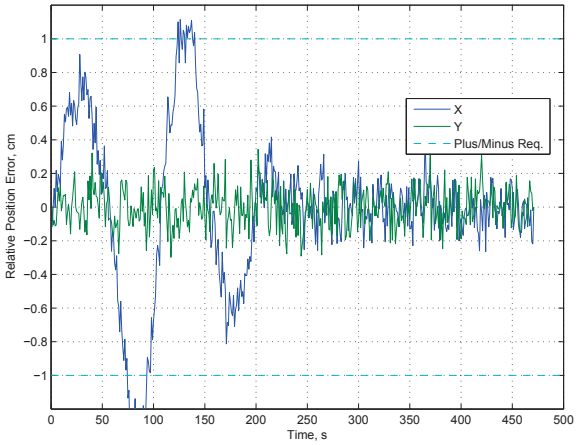

Figure 28. Simulated TPF-I Relative Position Error. After transient, $\pm 1\,cm$ performance met.

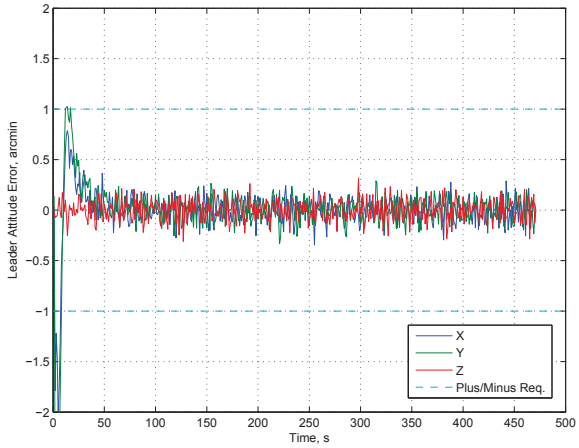

Figure 29. Simulated TPF-I Leader Attitude Error. After transient, $\pm 1\,arcmin$ performance met.

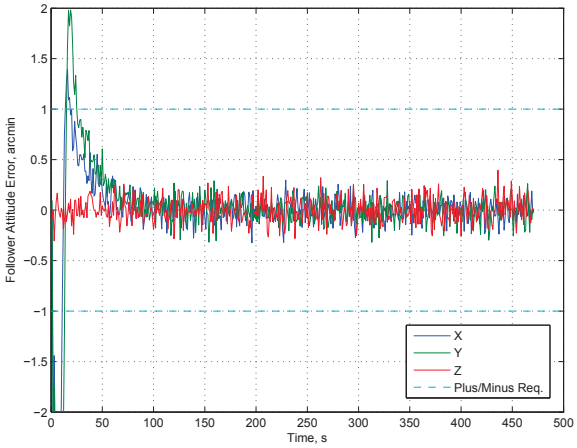

Figure 30. Simulated TPF-I Follower Attitude Error. After transient, $\pm 1\,arcmin$ performance met.

VI. Summary and Future Directions

A repeatable, robust capability for combined translational and rotational, synchronized precision formation flying has been demonstrated in a high-fidelity, flight-like ground environment for two vehicles. With the imminent installation of vertical stages, the robots of the Formation Control Testbed (FCT) can extend these ground demonstrations from 5DOF to 6DOF. The formation and attitude control system (FACS) algorithms are designed for 6DOF and an arbitrary number of spacecraft—although, in practice the computational requirements will become impractical for more than several tens of spacecraft. Nonetheless, *formation flying with coupled translational/rotational precision performance of better than* $5\,cm/6.7\,arcmin$ *has been demonstrated with flight-like dynamics, communication, actuation, and avionics.* The formation system is robust to communication drops and, based on high-level commands, able to execute precision 6DOF maneuvers with onboard formation path-planning and control.

There are several avenues for future work. In the near-term, the vertical stages will be integrated to provide the last translational degree of freedom and accelerometers are being investigated for real-time and compensation of floor slope. Also, a direct relative sensor, the Optical Pointing Loop, is being developed, which will allow demonstrations of sensor fusion for formation flying. In the longer term, the next step in formation complexity is to increase the number of vehicles. The Formation Algorithms and Simulation Testbed (FAST) is a distributed, real-time simulation environment.[17] Having demonstrated the FACS in the FCT, the FAST can now be validated against experimental data. With a validated simulation environment, many more spacecraft can be considered, and eventually, the FAST and FCT can be integrated to simulate tens of spacecraft with robots-in-the-loop capability.

VII. Acknowledgments

This work was conducted at the Jet Propulsion Laboratory, California Institute of Technology, under contract with the National Aeronautics and Space Administration.

References

[1]NASA Technical Translation, "A Brief Decription of the Radar Approach Equipment of the Soyuz-Type Spacecraft," November 1970. See also http://www.svengrahn.pp.se/histind/RvDRadar/IGLA.htm.

[2]Fehse, W., *Automated Rendezvous and Docking of Spacecraft*, Cambridge Univeristy Press, Cambridge, United Kingdom, 2003.

[3]Manno, V. and Page, D., editors, *Intercorrelated Satellite Observations Related to Solar Events*,Springer-Verlag, D. Reidel Publishing, New York, Dordrecht, 1969.

[4]Bristow, J., Folta, D., and Hartman, K., "A Formation Flying Technology Vision," *Proc. AIAA Space Conf.*, Long Beach, CA, 2000.

[5]Carpenter, K., Schrijver, C., Lyon, R., Mundy, L., Allen, R., Armstrong, T., Danchi, W., Karovska, M., Marzouk, J., Mazzuca, L., Mozurkewich, D., Neff, S., Pauls, T., Rajagopal, J., Solyar, G., and Zhang, X., "The Stellar Imager (SI) Mission Concept," *Future EUV/UV and Visible Space Astrophysics Missions and Instrumentation, SPIE Vol. 4854*, J.C. Blades and O.H.W. Siegmund, eds. 2003, pp. 293–302.

[6]Henry, C., "Terrestrial Planet Finder Interferometer 2005: overview of system design studies and technology development," *Techniques and Instrumentation for Detection of Exoplanets II, SPIE Vol. 5905*, edited by D. Coulter, 2005, pp. 1–7.

[7]Ticker, R. and Azzolini, J., "2000 Survey of Distributed Spacecraft Technologies and Architectures for NASA's Earth Science Enterprise in the 2010-2015 Timeframe," NASA Technical Memorandum, NASA/TM—2000-209964, NASA Goddard Space Flight Center, Greenbelt, MD, Aug. 2000.

[8]Battrick, ed., B., "X-ray Evolving Universe Spectroscopy—The XEUS Mission Summary," ESA-SP 1242.

[9]Fridlund, C., "Darwin—the Infrared Space Interferometry Mission," *ESA Bulletin*, Vol. 103, 2000, pp. 20–63.

[10]Ohkami, Y. and Kawano, I., "Autonomous rendezvous and docking by Engineering Test Satellite VII: A challenge of Japan in guidance, navigation and control," *Acta Astronautica*, Vol. 53, No. 1, 2003, pp. 1–8.

[11]Weismuller, T. and Leinz, M., "GN&C Technology Demonstrated by the Orbital Express Autonomous Rendezvous and Capture Sensor System," *Adv. Astro. Sciences Vol. 125: Gudance and Control 2006*, edited by S. Jolly and R. Culp, 2006.

[12]Brown, O. and Eremenko, P., "The Value Proposition for Fractionated Space Architectures," *AIAA Space Conf.*, x, 2006.

[13]Lawson, P. and Dooley, J., "Technology Plan for the Terrestrial Planet Finder Interferometer," JPL Publication 05-5, Jet Propulsion Laboratory, California Institute of Technology, Pasadena, CA, USA, 2005, Available online at http://planetquest.jpl.nasa.gov/Navigator/library/tpfI414.pdf.

[14]Regehr, M., Acikmese, A., Ahmed, A., Aung, M., Clark, K., MacNeal, P., Shields, J., Singh, G., Bailey, R., Bushnell, C., Hicke, A., Lytle, B., and Rasmussen, R., "The Formation Control Testbed," *Proc. IEEE Aerospace Conf.*, Big Sky, MT, 2004, pp. 557–564.

[15]Scharf, D., Hadaegh, F., Keim, J., Benowitz, E., and Lawson, P., "Flight-like Ground Demonstration of Precision Formation Flying Spacecraft," *Proc. SPIE Vol. 6693.*, 2007, pp. 669307.1–12.

[16]Scharf, D., Hadaegh, F., Rahman, Z., Shields, J., Singh, G., and Wette, M., "An Overview of the Formation and Attitude Control System for the Terrestrial Planet Finder Interferometer," *Proc. 2nd Int. Symp. on Formation Flying Missions & Technologies*, Washington, D.C., 2004.

[17]Wette, M., Sohl, G., Scharf, D., and Benowitz, E., "The Formation Algorithms and Simulation Testbed," *Proc. 2nd Int. Symp. on Formation Flying Missions & Technologies*, Washington, D.C., 2004.

[18]Ruth, M. and Tracy, C., "Video-guidance design fro the DART rendezvous mission," *Proc. SPIE Vol. 5419: Spacecraft Platforms and Infrastructure*, edited by P. Tchoryk, Jr. and M. Wright, 2004, pp. 92–106.

[19]Purcell, G., Tien, J., Young, L., and Srinivasan, J., "Formation Acquisition Sensor for the Terrestrial Planet Finder Mission," *Proc. IEEE Aerospace Conf.*, Big Sky, MT, 2004.

[20]Scharf, D., Hadaegh, F., and Ploen, S., "A Survey of Spacecraft Formation Flying Guidance and Control (Part II): Control," *Proc. Amer. Contr. Conf.*, Boston, MA, 2004.

[21]Beard, R., McLain, T., and Hadaegh, F., "Fuel Optimization for Constrained Rotation of Spacecraft Formations," *J. Guid., Contr., & Dyn.*, Vol. 23, No. 2, 2001, pp. 339–346.

[22]Singh, G. and Hadaegh, F., "Collision Avoidance Guidance for Formation-Flying Applications," *Proc. AIAA Guid., Nav.,& Contr. Conf.*, Montreal, Canada, 2001.

[23]Martin, S., Scharf, D., Wirz, R., Lay, O., McKinstry, D., Mennesson, B., Purcell, G., Rodriguez, J., Scherr, L., Smith, J.R., and Wayne, L., "Design Study for a Planet-Finding Space Interferometer," *Proc. IEEE Aerospace Conf.*, Big Sky, MT, 2008.

[24]Sengupta, A., Anderson, J. R., Brophy, J. R., Kulleck, J., Garner, C. E., deGroth, K., Karniotis, T., Banks, B., and Walters, P., "The 30,000-Hr Life Test of the DS1 Flight Spare Ion Thruster, Final Report," Tech. rep., NASA T/TP 2004-213391, 2004.

A. Performance for Remaining Demonstrations

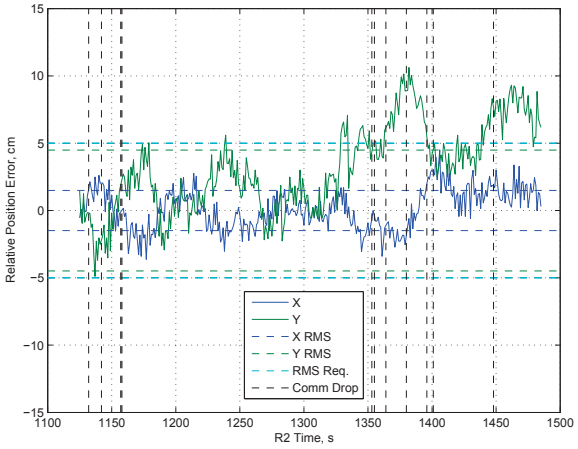

Figure 31. Formation Error for Demonstration 1.

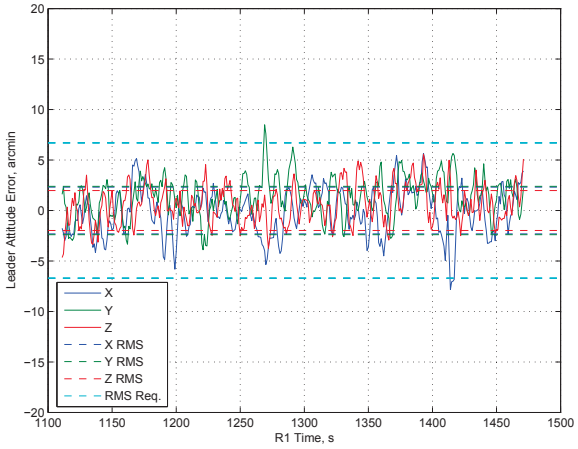

Figure 32. Leader Attitude Error for Demonstration 1.

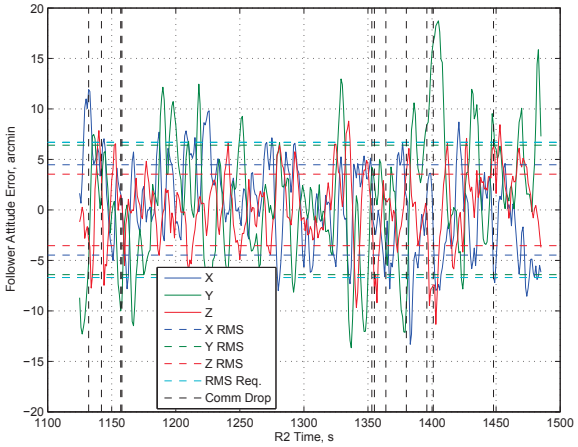

Figure 33. Follower Attitude Error for Demonstration 1.

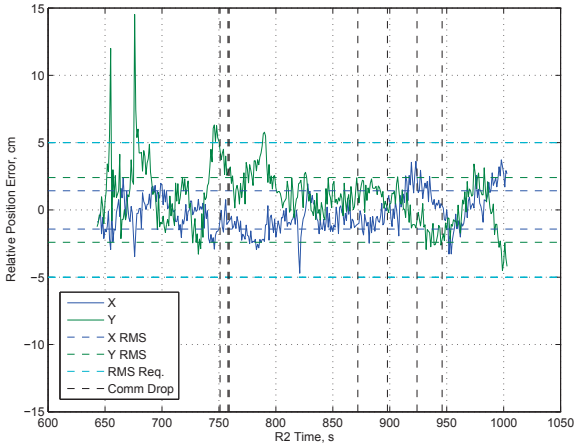

Figure 34. Formation Error for Demonstration 2. Sensor error spikes at approximately $640\,s$ and $660\,s$.

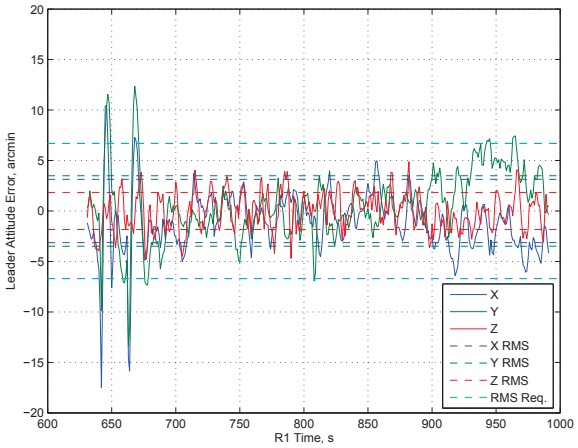

Figure 35. Leader Attitude Error for Demonstration 2. Sensor error spikes at approximately 640 s and 660 s.

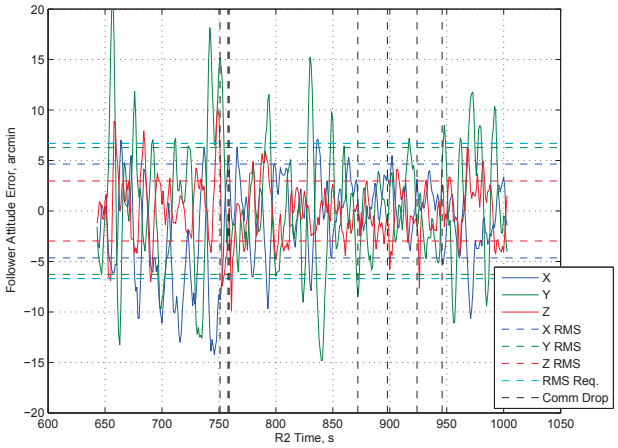

Figure 36. Follower Attitude Error for Demonstration 2.

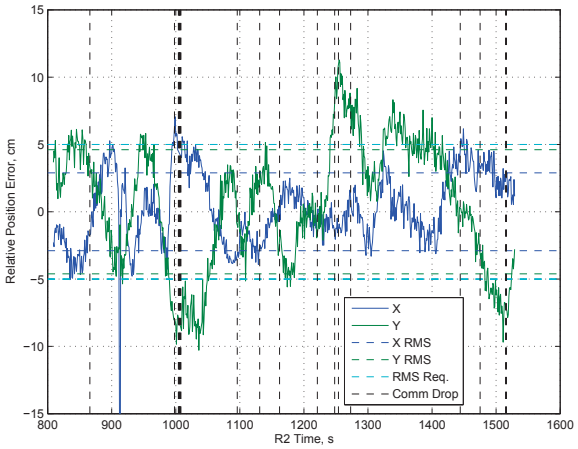

Figure 37. Formation Error for Demonstration 4. Sensor error spike at approximately 910 s.

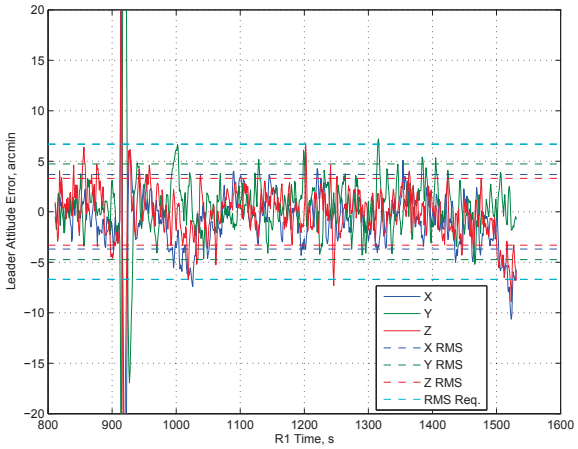

Figure 38. Leader Attitude Error for Demonstration 4. Sensor error spike at approximately 910 s.

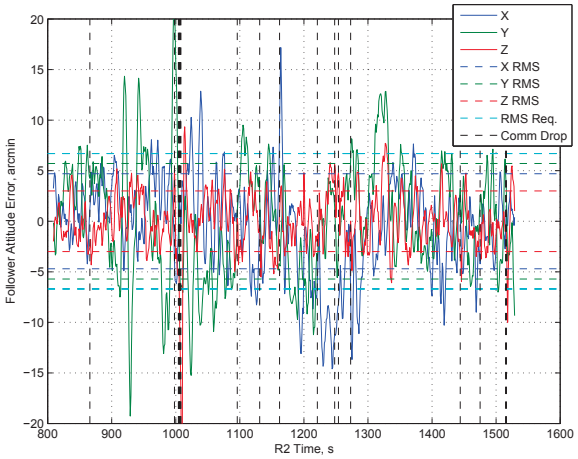

Figure 39. Follower Attitude Error for Demonstration 4.

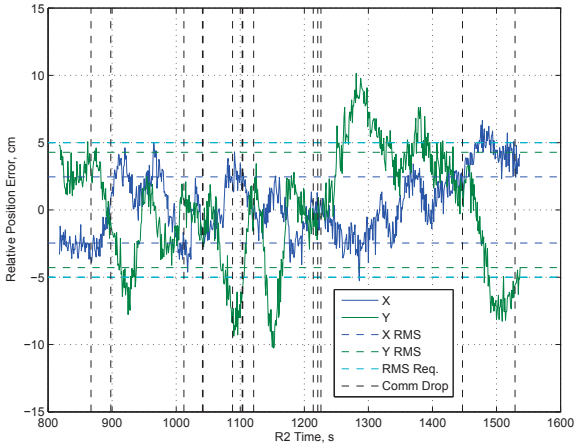

Figure 40. Formation Error for Demonstration 5.

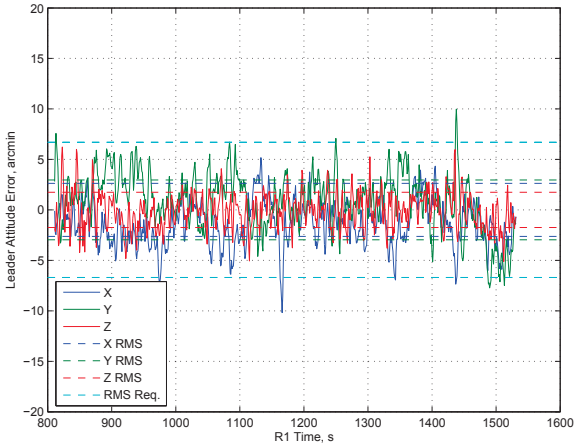

Figure 41. Leader Attitude Error for Demonstration 5.

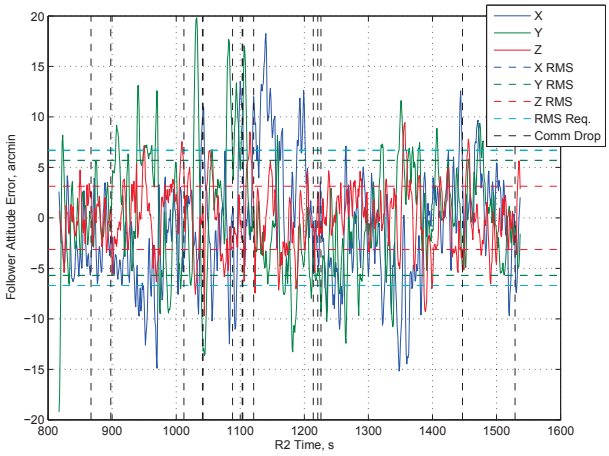

Figure 42. Follower Attitude Error for Demonstration 5.

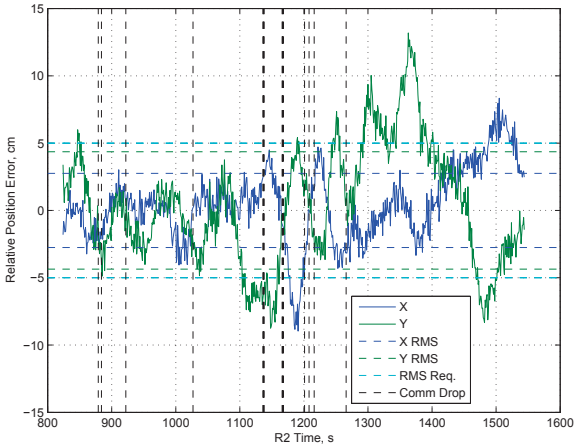

Figure 43. Formation Error for Demonstration 6.

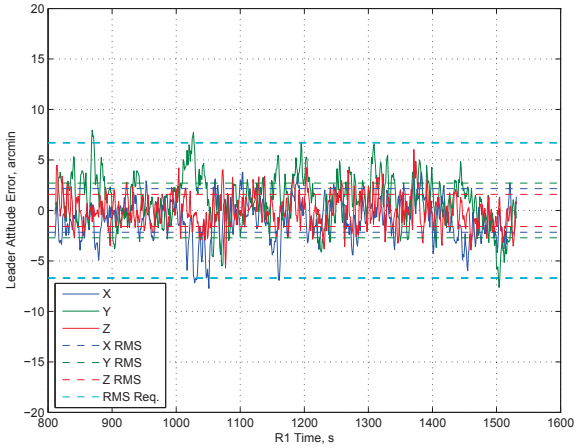

Figure 44. Leader Attitude Error for Demonstration 6.

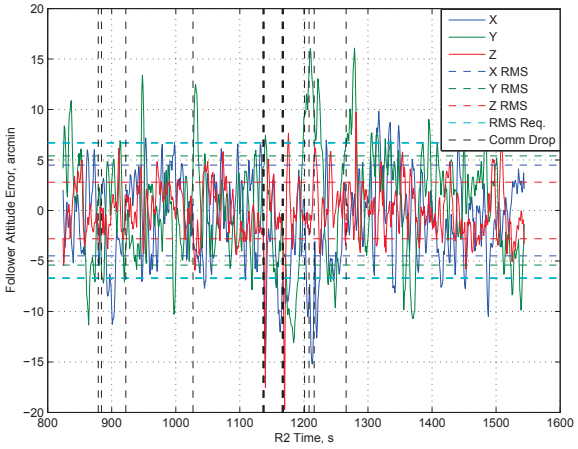

Figure 45. Follower Attitude Error for Demonstration 6.